

DYNAMIC MODELING FOR STRUCTURES  
WITH BOLTED JOINTS

By

Asal Kharazi Kalajahi

Thesis

Submitted to the Faculty of Mechanical Engineering  
At Politecnico di Torino

for the degree of

MASTER OF SCIENCE

in

Mechanical Engineering

March-April 2019

## CONTENTS

Introduction .....	3
What is a jointed structure? .....	3
Modeling of Mechanical Joints .....	3
Commercial codes.....	4
What is a common joint? .....	4
Historical Development .....	4
The benefit of designing structures with Joints.....	6
Perspectives for the Economics of Jointed Structures: .....	6
Experimental Techniques for Studying Energy Dissipation Mechanics .....	6
Round Robin Systems.....	6
Damping.....	20
The damping sites within a bolted joint .....	20
Considerations for Measurements of Jointed Structures .....	21
Effects of Experimental Setup.....	21
Best Practices for Experiments on Jointed Systems .....	21
Introduction of constitutive models .....	22
Modeling Considerations .....	22
Friction Models .....	22
1.Velocity-Based Models.....	22
2. State-Based Models .....	23
Test case: Two Cantilevered Beams.....	26
RESULTS .....	27
Case study Beam 1 .....	27
Case Study Beam 2.....	29
Case Study of Two Cantilever Beams Assembly with four bolts.....	32
Iwan Model Introduction .....	37
Four-Parameter Iwan Model .....	38
Extended Iwan-Type Models: Five-Parameter Iwan-Type Model .....	42
The Next Generation of Joints Research.....	44
On Numerical Modeling.....	44

## INTRODUCTION

### What is a jointed structure?

The primary function of a joint in an engineering structure is to connect, usually stiffly, two (or more) separate substructures. Joints introduce two features to a structure: amplitude dependent stiffness and amplitude dependent damping. The amplitude dependent stiffness can be predicted reasonably well (to within 10%); however, the amplitude dependent damping is still beyond predictive capabilities. The analysis of jointed structures consists of two principle parts: the deterministic/linear substructures that can be readily modeled and analyzed with existing techniques, and the often unpredictable assembly of a jointed structure that exhibits emergent behavior not observed in the deterministic substructures.

In joint mechanics, contrary to Hayek's assertion, it is quite possible that the knowledge for fully characterizing a joint will be prohibitively difficult to obtain for modeling purposes. From experimental and numerical evidence, the nonlinearities introduced by joints seem to be dependent upon qualities introduced by the manufacturing process that cannot be measured.

### Modeling of Mechanical Joints

As of yet, there is no consensus for the best practice of modeling a jointed connection. In academia, there are many new techniques that are often in their infancy: significant validation and verification work is needed in addition to making them usable and efficient.

The analysis is divided into three stages:

1. Nonlinear Static Solve
2. High Fidelity Contact Interface Modeling
3. Dynamic Analysis

The first step, the nonlinear static solve, is used to determine which nodes in the interface are stuck together, and which nodes are not expected to be in contact.

In the second step, the problem is reduced slightly by assuming that nodes that are out of contact will remain out of contact during the analysis. The remaining nodes are considered to be potentially slipping. Though under certain circumstances these could be divided into stuck and slipping, in which case the stuck nodes just need to be attached with linear springs.

The third step is the dynamic analysis. Once the contact interface has been prescribed, the next challenge is determining the quantity of interest. For frequency responses, harmonic balance-based simulations are preferable as the frequency response will exhibit nonlinearities dependent up on the excitation amplitude.

## Commercial codes

Large number of node-to-node contacts will need to be specified for high fidelity finite element commercial codes. Recent advances by commercial finite element packages exhibit capabilities to minimize the burden placed on the user for this modeling. some successful commercial codes to mention are:

- The use of ADAMS, a multibody dynamics code, with flexible bodies modeled in NASTRAN (Hopkins and Heitmann 2016). This approach is very efficient for macroslip, but not amenable for microslip applications.
- The use of ANSYS to introduce bolts to geometrically flat surfaces.
- The use of ABAQUS, Hyperworks, or other codes with node-to-node contact and preloaded bolts.

The goal of joint research is, and will continue to be for the foreseeable future, the development of a predictive model for the interfacial dissipation and stiffness of a joint.

## What is a common joint?

It is defined as the mating of two components through a bolted connection. This simple geometry is used in wind turbine structure and cylindrical flanges or seals. The lap joint is the most common type of interface found in built-up structures. Throughout all of the perturbations of the simple lap joint geometry, the common features are one (or more) bolts used to hold together two (or more) surfaces under a normal compressive load due to the bolt.

In general, lap joints are designed such that the compressive load is sufficiently high to prevent the massive relative motion of the two components. Movement along the interface between the two components is generally isolated and not complete throughout. This isolated movement is termed microslip and specifically refers to the relative motion between the two interfaces that only occurs over part of the interface while the rest of the interface exhibits no relative motion. Microslip is expected to first occur away from the bolt locations. As the excitation magnitude is increased, the domain of microslip will increase until the entire interface exhibits relative (sliding) motion, which is macroslip.

In designing a lap joint, the primary function is to connect stiffly two components. This task is relatively straightforward, and there are multiple handbooks that detail selections of materials, bolts, and preload to ensure that the primary function of a joint is met.

## Historical Development

Taking into consider the immense nature of the challenge of developing a predictive model of friction, the American Society of Mechanical Engineers (ASME) Research Committee on the Mechanics of Jointed Structures was formed to develop collaborations and to advance the state of the art for modeling structures with jointed interfaces. As part of the collaborations established by this community, a series of workshops have been conducted over the past eight years (Segalman et al.2007, 2010; Starr et al.2013). At the

conclusion of these workshops, the last activity is to summarize the discussion and to formulate a series of challenges and action items.

From the first workshop ( Segalman et al. 2007), three challenges were identified:

- 1.The experimental measurements of joint properties
- 2.Interface physics
- 3.Multi-scale modeling

These three challenges represent an ambitious set of goals that have persisted into the outcomes of the subsequent two workshops. One direct consequence of this workshop was the publication of the Joints Handbook (Segalman et al.2009), which methodically detailed Sandia National Laboratories' approach to experimental measurements and numerical modeling of joints in structures. This handbook has since been used extensively by the joints community.

The second workshop (Segalman et al. 2010) built on the set of challenges formulated during the first workshop and defined eleven new challenges:

1. Round-robin/benchmark exercise for hysteresis measurements
2. Round-robin/benchmark exercise for the measurement and prediction of dissipation in standard joints
3. Repeatability and variability
4. Framework for multi-scale modeling
5. Strategy for uncertainty and nonlinearity
6. Methodology to quantify the cost benefits of improved joints designs
7. Universally accepted physical theory of friction
8. Complex loading strategies
9. Measurement of spatial distribution of key physical parameters
10. How to include surface chemistry?
11. Eventual implementation of prediction methods in commercial numerical codes

Inherent in this set of eleven challenges are the same three themes from the first workshop: experimentally measuring joint properties, the physics of the joint interface, and modeling techniques to bridge the gap between reality and simulation. The modeling techniques can be subdivided into three overarching classes: multi-scale frameworks, uncertainty quantification and propagation, and numerical methods to simulate a jointed system efficiently and accurately. The three themes are seen again with the challenges developed at third workshop.

From the third workshop, seven challenges were defined after a mini-workshop held the following year revisited them. These challenges are:

1. Round-robin/benchmark exercise for hysteresis measurements
2. Round-robin/benchmark exercise for measurement and prediction of dissipation in standard
3. The economics of jointed structures
4. Defining the mechanism of friction
5. Epistemic and aleatoric uncertainty in modeling and measurements
6. Derivation of constitutive equations based on physical parameters
7. Eventual implementation and integration of prediction methods in finite element codes

Following the third workshop and before the mini-workshop which was held in Portland, five other challenges existed: modeling nonmetallic interfaces, multi-scale modeling framework, epistemic and aleatoric modeling, definition of variability and uncertainty, and time varying model parameters, modeling and experimental “surface chemistry”. The challenge on modeling nonmetallic interfaces was postponed in order to focus our efforts on metallic interfaces first before considering a second class of interfaces.

## **The benefit of designing structures with Joints**

Engineers and designers can directly reduce the cost by reducing the number of man-hour needed to design a system with the use of joints in the models and the handbooks with easily digested metrics for how a specific joint performed.

One goal of joints research is to be able to use joints to monitor the state of a structure actively. With this capability, it would be possible to plan a repair cycle optimally for a given structure, and to then use the joints as an early warning sign to help avoid a structural failure. Thus having joints as a means of detection of potential problems could introduce significant cost savings. This is particularly relevant to the aerospace industry.

Perspectives for the Economics of Jointed Structures:

The economics of joints is an issue central to not on the direction of research for interfacial mechanics, but also for the design and development of complex structures. In order to motivate the central tenet of economics of jointed structures properly, a cost benefit analysis of joints is needed.

If a better understanding of joints existed such that load transmissions, fatigue, and failure could be better predicted, then this would avoid costs associated with failures.

In context, the USA has 7185 commercial aircrafts in service (Karp 2012), Every kilogram saved on joints would have a potential to save approximately \$1 million per year in fuel costs (given the average lifetime of a commercial aircraft is approximately 20 years).

Every year, it is estimated that over \$2.5 billion is spent on the model and dynamic testing of systems (specifically, vibration tests account for approximately \$2 billion annually) (Sakion 2014). The order of \$200 million annually could be saved or significantly reduced for testing expenditures by a better understanding of joint behavior (Brake et al.2016).

## **Experimental Techniques for Studying Energy Dissipation Mechanics**

### **Round Robin Systems**

The goal of the round robin benchmark challenge for measurement and prediction of dissipation in standard joints is to develop a methodology and a suitable system to both measure and predict the dissipative behavior of joints in built-up structures.

Due to the lack of understanding of how joints dissipate energy, much of the design of benchmark systems has involved some trial and error. Only recently have designs been put forth that appear suitable to address both of the difficulties listed:

1. The system may or may not have adequately nonlinear behavior due to the influence of the joints, the surrounding structure, and other factors.
2. Many systems that have realistic behaviors often have qualities that make modeling more complex than a benchmark aims to be.

Several qualities important for developing systems to study joint mechanics have also been identified in Segalman et al. (2009):

1. Well controlled and understood boundary conditions
2. Simple experimental setup
3. Design of experiments with behavior that can be understood by engineering analysis.

### *The Brake-Reuß Beam*

The Brake-Reuß beam is a set of three beams, shown in figure 1. that are designed to study the influence of a lap joint on a system's dynamics. In all three cases, the first version of system is 72 cm long with a 2.5 cm square cross-section (more recent versions have slightly different dimensions due to being manufactured in the USA where stock material is available in common English units instead of in Germany where stock material is available in common metric units). For both the monolithic beam with three bolts and the jointed beam, the bolt-holes are 0.85 cm in diameter, and located approximately along the beam's centerline. All of the beams are fabricated from ASTM A283 steel, with 5 cm long M8 bolts. Between the bolt head and the beam, and between the nut and the beam on the other side of the bolt, are 0.3 cm thick washers with a 2.1 cm outer diameter and 0.8 cm inner diameter. The first beam is a monolithic beam with no frictional interfaces, which is used as a control to study the effect of both the bolts and lap joint. The second beam in figure 1. is identical to the monolithic beam with the exception of three through holes. This second beam is designed to quantify the effects of bolts themselves. The third beam in figure 1. consists of a lap joint that is held together via three bolts.

This benchmark system has been extensively analyzed at the Nonlinear Mechanics and Dynamics (NOMAD) Research institute, hosted by Sandia National Laboratories (Brake et al. 2015)

Current research on the Brake-Reuß beam is focused on:

1. Characterizing the distribution of parameters to describe models representing the jointed interface (Bonney et al.2016);
2. Developing high fidelity and reduced order models of the system (Grob et al.2016)
3. Further investigation of the application of linear methods to study this nonlinear system (Catalfamo et al. 2016)
4. Studying how different types of stress waves propagate across the lap joint interface (Flicek et al.2016)
5. Measuring the effects of geometric changes to the interface (Dossogne et al.2017)

6. Assessing the effects of the far-field structure on the measured joint properties (Rosatello et al.2017)

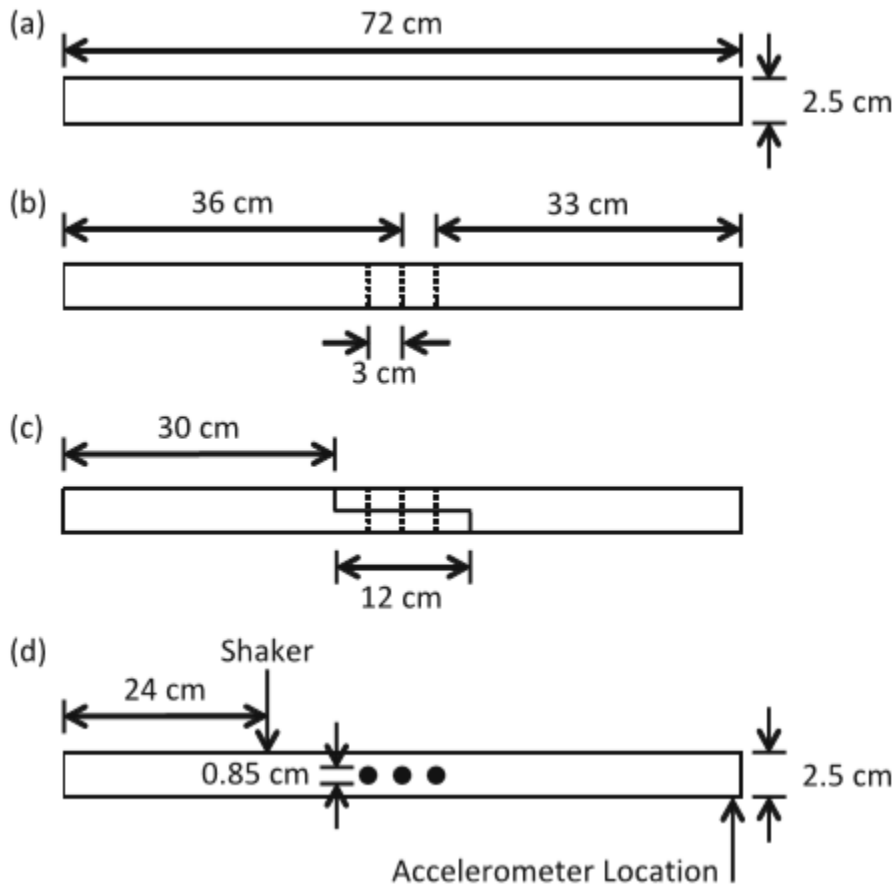


**Figure 1.** The geometry of the (a) monolithic system, (b) monolithic system with bolt holes, (c) jointed system and (d) top view of the monolithic system with bolt holes. For both the monolithic system with bolt holes and the jointed system, the size and position

### Experimental Evidence of Variability for the Brake-Reuß Beam

For the monolithic beam, the natural frequencies and damping ratios are independent of load level. For the jointed system, the natural frequencies and damping ratios both varied with bolt preload, order in which the bolts are tightened, and excitation level as discussed in what follows. The response of all three systems is measured with an accelerometer located at the corner of the beam farthest from the stinger/shaker attachment point. For the monolithic beam, transfer functions are also calculated between the response point and 52 excitation points on the beam in order to identify and visualize the mode shapes for the system via impact hammer tests. For consistency, a shaker attached to the beams via a stinger is used to excite the beams for all subsequent FRF measurements

The FRF for both the monolithic beam and the monolithic beam with bolts is shown in figure 2. The presence of the through-holes is shown to decrease the natural frequencies slightly (between 1 and 3.5%) for the bending modes and first torsional mode. The shift in natural frequencies is more pronounced for

the second torsional mode, located near 4 kHz. This trend persists at higher frequencies as well: the bending modes change in frequency by less than 2%, and the torsional modes differ by increasingly larger percentages. Natural frequencies and damping ratios for all 3 beams are detailed in table 1.

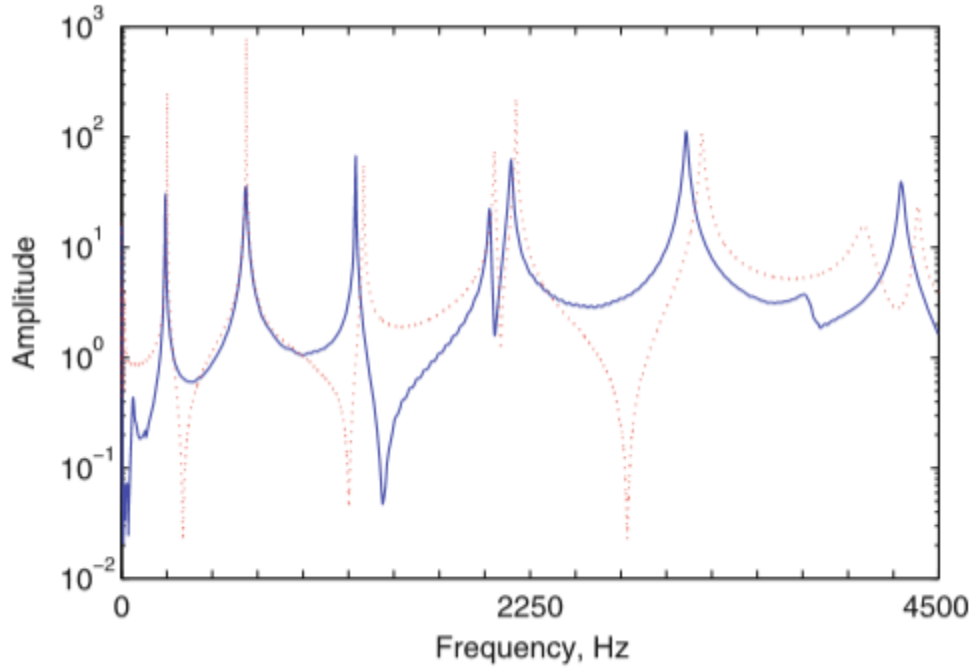


**Figure 2.** Frequency response function (FRF) for the monolithic beam (dotted line) and the monolithic beam with bolts tightened to 10 Nm (solid line)

**Table 1.** Natural frequencies for the three different beams at an excitation amplitude of 0.1 N

Mode	Monolithic		Monolithic with bolts tightened to 10 Nm		Jointed with bolts tightened to 4 Nm	
	Natural freq. (Hz)	Damping ratio (%)	Natural freq. (Hz)	Damping ratio (%)	Natural freq. (Hz)	Damping ratio (%)
Bending 1	251.4	0.0594	242.7	0.0991	240.6	0.0933
Bending 2	687.4	0.0358	685.4	0.0505	684.1	0.1098
Bending 3	1333.1	0.1199	1290.9	0.1840	1284.0	0.2658
Bending 4	2172.1	0.1216	2146.3	0.3198	2115.6	0.2692
Bending 5	3196.4	0.2848	3118.2	0.3560	3105.0	0.2026
Bending 6	4385.4	0.2374	4307.3	0.2958	4281.5	0.2147
Torsional 1	2053.1	0.1672	2027.9	0.2313	2018.7	0.3854
Torsional 2	4093.0	1.1047	3778.5	0.6863	3799.1	1.0207

**Table 2.** Natural frequencies for the three different beams at an excitation amplitude of 0.1 N and 2 N

Mode	Monolithic with bolts tightened to 10 Nm		Jointed with bolts tightened to 10 Nm	
	0.1 N excitation	2 N excitation	0.1 N excitation	2 N excitation
Bending 1	242.7	242.7	181.2	180
Bending 2	685.4	685.4	605.0	605.0
Bending 3	1291	1291	1200	1199
Bending 4	2146	2146	1738	1733
Bending 5	3118	3118	2937	2929
Bending 6	4307	4307	3940	3943
Torsional 1	2028	2028	1680	1678
Torsional 2	3779	3779	2999	2998

The monolithic beam with bolts does not exhibit any strong nonlinear behavior. Figure 3 presents the FRFs of the monolithic beam with bolts at four different excitation levels (0.1, 0.5, 1, and 2 N). Aside from the small deviation near 1kHz, which could be an artifact of the shaker or stinger attachment, the response is effectively the same at all excitation levels. By contrast, for the jointed system, the natural frequencies decrease by up to 0.3% over the same excitation range (with the exception of the sixth bending mode, which exhibits a stiffening behavior). As detailed in Table 2.

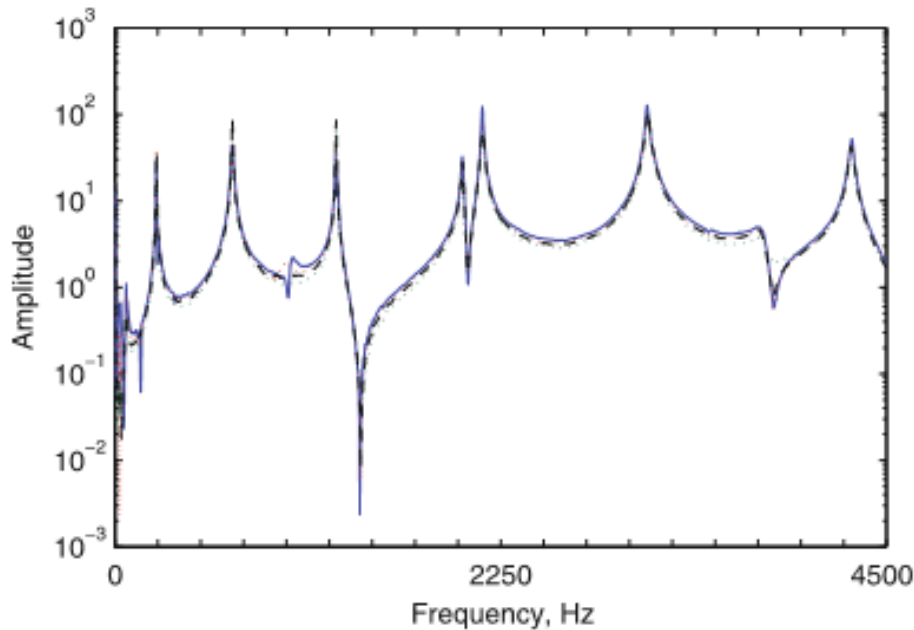


**Figure 3.** FRF for the monolithic beam with bolts at four different excitation levels and bolts preloaded to 10 Nm

The jointed system shows a high degree of variability, as is evident in figure 4, which is indicative of a strong nonlinearity. In all experiments involving the jointed system, unless otherwise noted, the excitation amplitude is 0.1

N. Figure 4 presents the FRF of the system for a preload of 20 Nm on each bolt across multiple assemblies and three different orders of the bolt being tightened. The bolts are tightened only once per assembly as preliminary measurements indicated that there is no loss of preload during a test.

The natural frequencies and damping ratios for bending modes are relatively consistent. The torsional modes (near 3.5, 4.2, and 5.7 kHz), however, change in frequency and damping ratio each time the system is reassembled (whether the bolts are tightened in the same order or not). This result indicates that the torsional modes are more sensitive to the interface conditions (such as alignment, roughness, etc.), and the bending modes are more sensitive to the order in which the bolts are tightened. The order in which the bolts are tightened is posited to be directly related to differences in residual stresses between each assembly.

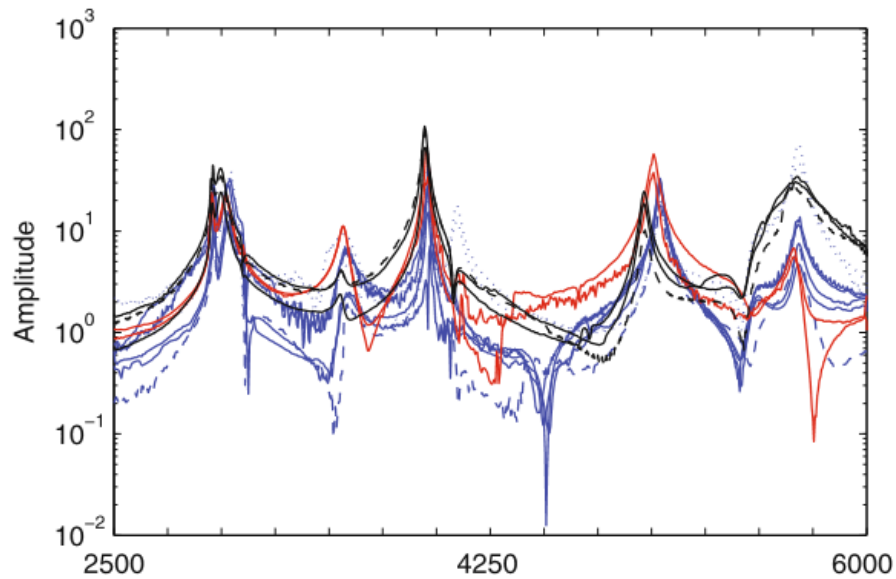


**Figure 4.** FRF for jointed beam with bolts tightened to a preload of 20 Nm. The different color lines correspond to different orders in which the bolts were tightened, and the (solid) and (dashed) lines correspond to different assemblies of the system under the same conditions

At lower preloads the bending modes (at 1.2 and 1.7 kHz in figure 5) is varied significantly in frequency and slightly in terms of damping ratio. As the system is disassembled and reassembled using the same order of bolt tightening (having a similar residual stress field), the natural frequencies and damping ratios of the bending modes remain consistent, though the amplitude of the response is observed to change.

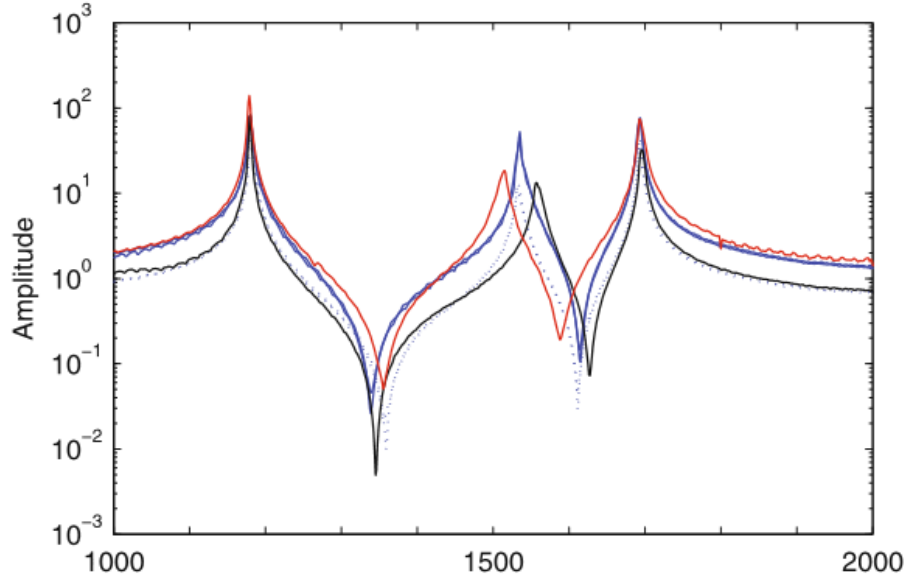


**Figure 5.** FRF for the jointed beam with bolts tightened to a preload of 5 Nm. The different color lines correspond to different orders in which the bolts were tightened, and the (solid) and (dashed) lines correspond to different assemblies of the system under the same conditions

As the preload of the bolts is increased to 40 Nm, shown in figure 6, the natural frequencies and damping ratios are observed to remain approximately constant across reassembly for both the torsional mode (at 1.75 kHz) and the bending modes. This implies that the preload is sufficiently high enough, relative to the excitation level at least, for the system to behave linearly.

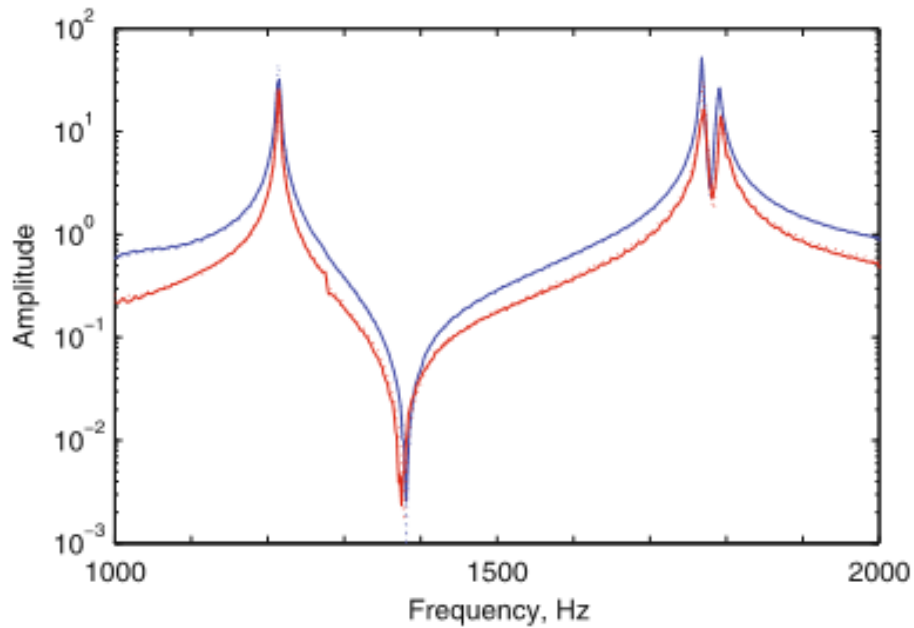


**Figure 6.** FRF for the jointed beam with bolts tightened to a preload of 40 Nm. The different color lines correspond to different orders in which the bolts were tightened, and the (solid) and (dotted) lines correspond to different assemblies of the system under the same conditions

Resulting from the previous observation:

- One class of modes (bending modes) are sensitive to the residual stresses in the system (as correlated to the order in which the bolts are tightened)
- A second class of modes (torsional modes) are so sensitive to the interfacial conditions that the effect due to the residual stresses is not distinguishable from other effects

### *The Square, Four-Bolt Plate*

A second benchmark system that has recently been proposed is a square, four-bolt plate. This system, which consists of two square plates bolted together by four bolts (one located in each corner), exhibits significantly more damping than a monolithic structure of the same dimensions. Due to its ease of fabrication and damping characteristics, this system is a good candidate for modeling. Unlike the Brake-Reuß beam, which has a large, distributed contact surface, the square, four-bolt plate's contact patches are reduced to the area of washers located between each plate; While the configuration without washers has been used, this introduces an additional nonlinearity due to the plates slapping. Previous iterations of this system have determined that a six-inch plate is able to produce richer dynamics than observed in smaller (four inch and five inch) plates. Preliminary analysis of this system is detailed in Segalman et al.2015.

The system exhibits several strong nonlinearities:

1. For multiple configurations, the amplitude dependent damping characteristics common to jointed structures is observed.
2. When the plates are assembled without washers, an additional nonlinearity due to the plates slapping is observed.
3. The dissipation indicates a strong dependence on the spatial location of the excitation that is atypical of linear systems.
4. A final source of nonlinearity is hypothesized to be the two plates moving opposite one another for several nodes (as opposed to moving in the same direction at all times). This has significant ramifications for the modeling of the local kinematics at the bolt locations.

Thus, this system presents some rich set off nonlinearities to study for advancing the development of a round robin system; however, the one drawback is that the joints that constitute this system are not representative of real structure.

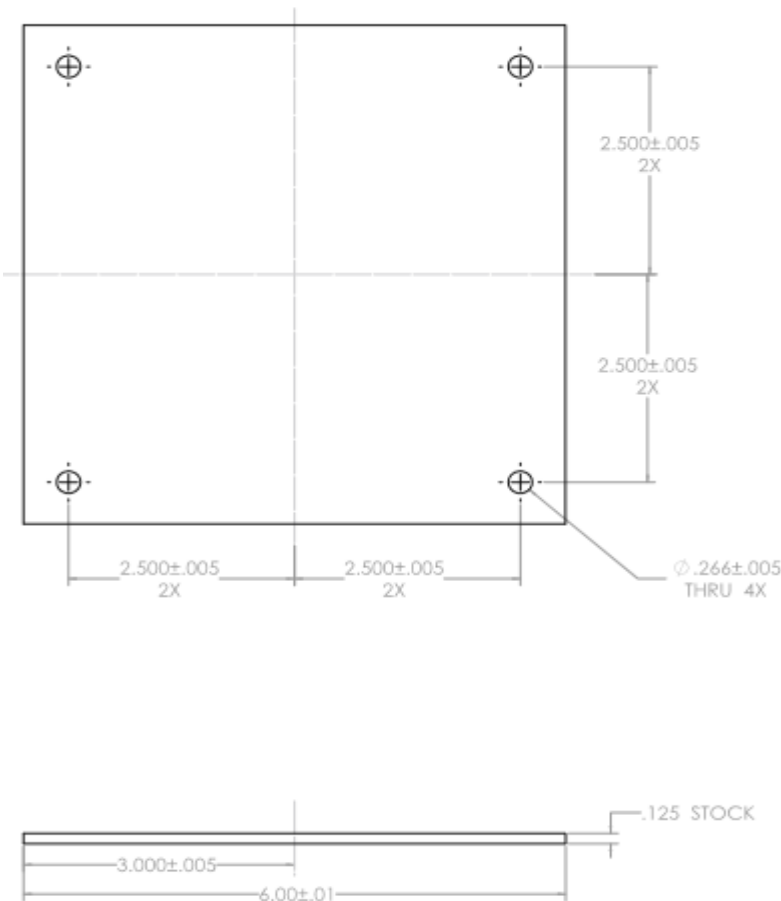


**Figure 7.** The geometry of the square, Four-Bolt Plate structure from top and side view

### *The Gaul Resonator and Dumbbell Apparatus*

The Gaul Resonator (Gaul et al.1994) features a single bolt lap joint that connects two monolithic structures, one of which is designed to have a stiffness element in it (Fig.8.a). This has the advantage of allowing for large dynamic loads to be transmitted to the interface. Similar structures, such as the dumbbell oscillator (Segalman et al.2009) (shown in Fig.8.b; does not include a stiffness element), are typically designed to be massive for the natural frequencies of the structure to be relatively low, which is beneficial for developing measurements with minimal noise and high resolution). The large dynamic loads transmitted across the joint facilitate the study of the transition from microslip to macroslip, even with clamping forces or preloads that are representative of industrial applications. The benefit that massive structures have is that effects due to the attachment of sensors and excitation sources are negligible, the

boundary conditions are able to be better controlled, and large amounts of energy are able to be stored in the structure for extensive ring-down testing. Further, due to the massive design and the relatively low compliance of the joint, the structure is able to be modeled accurately with a low order discrete mass representation featuring a nonlinear element in the location of the joint.

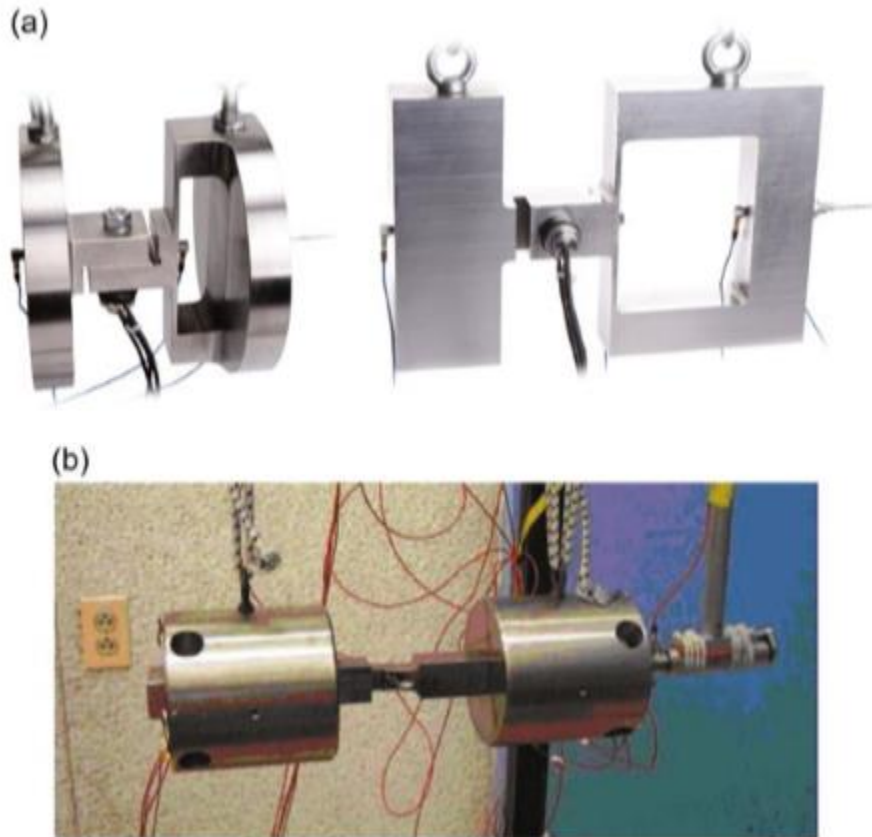


**Figure 8.** (a) Two examples of Gaul resonator, and (b) the Dumbbell apparatus

In measuring the behavior of jointed structures, it is often difficult to isolate the nonlinear behavior of one bolted joint from other disturbing effects resulting from support structure. This system is an ideal benchmark for measuring the transfer behavior of a bolted lap joint and also delivers the opportunity to perform hysteresis measurements, which establishes a bridge between the two round robin challenges. The basic design is related to the so-called dumbbell oscillator Segalman et al. (2009), consisting of two steel masses connected by a lap joint (Fig.9)

Since the axial resonance frequencies of this arrangement lie in a quite high frequency range, the setup is modified by a relatively soft spring, as illustratively shown in (fig.9)

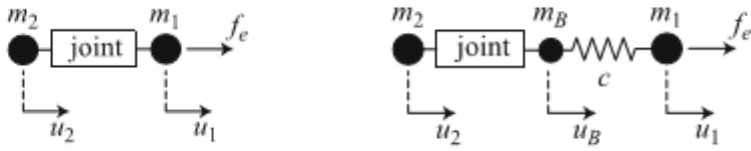


**Figure 9.** Principle dumbbell oscillator and on the right side the Principle resonator setup

This operation mode of the oscillator also leads to the designation of being a “resonator” Two different types of such resonators were developed at the University of Erlangen-Nurnberg. The first one is made of round stock stainless steel and has a similar geometry and equal dimensions like the ones investigated in Gaul and Bohlen (1987) and Lenz and Gaul (1995). The second one is an improved version made of flat stock material and a different orientation of the lap joint.

The parts of the systems were manufactured from solid material and are therefore monolithic. The spring is designed in the form of a thin bending spring (Fig.10).

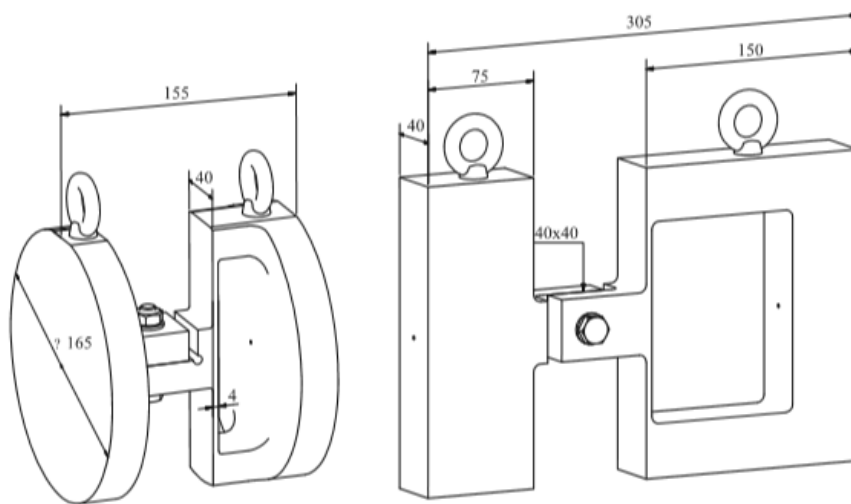


**Figure 10.** Resonator drawings

### *The Cut Beam Frictional Benchmark System*

The Cut Beam Frictional Benchmark System is a clamped-clamped beam excited on its first bending mode. The beam (fig.5.3) is built up with three parts linked by two frictional interfaces. A normal pre-load is applied to both extremities of the beam before they are clamped to the ground. Due to the pre-load, the three parts remain in contact even during the bending motion. This design minimizes coupling between pre-load induced normal stresses in the planar joints and the vibration-induced shear stresses due to the zero bending moment at the location of the joints. The beam is a revision of a previous experiment (Peyret et al.2010), and is developed with several advantageous features. The shape of the beam is designed to maximize damping by having large interface areas, and is designed to minimize coupling between the

normal stresses and the vibration motion even in the case where the interfaces are located imprecisely. Despite the form differing from that of a bolted assembly, this benchmark system reproduces the loading conditions of an assembly under constant normal load.

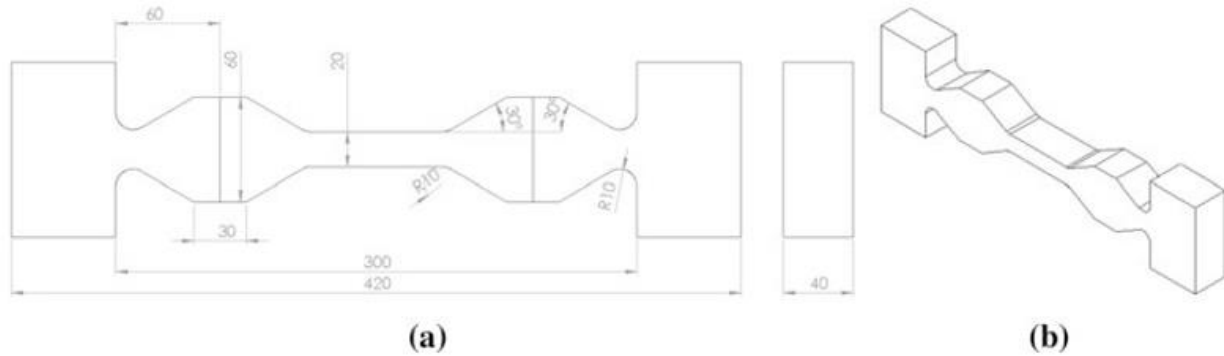


**Figure 11.** The SUPMECA frictional benchmark system: **(a)** geometry and **(b)** isometric view

### *The Ampair 600 Wind Turbine (page 63)*

The Ampair 600 wind turbine is one of the candidate systems and a commercially available system for the round-robin for dissipation measurements and prediction challenge. The Ampair 600 wind turbine was the first true benchmark system for the current generation of research challenges as it has been studied widely and shared amongst a number of different institutions. It is not an academic system but rather a real application. The same system is already being used as the selected test bed for Dynamics Substructuring Focus Group.

Each substructure (e.g., the blades or the hub) is not a monolithic structure. The blades are composed of composite materials and foam, and the central hub is potted with epoxy amongst other materials. In other words, accurate modeling of the system requires material models that include viscous and plastic behavior. While some methods exist to characterize this system in linearized portions of its domain, it is a more complicated system to use as a benchmark than either the Brake-Reuß beam or the Square, Four-Bolt Plate. Another challenge that has become evident in analyzing the Ampair 600 Wind Turbine is that due to the construction method, the measurement of the joint properties exhibits a higher degree of variability than observed in other benchmark systems.



**Figure 12.** The Ampair 600 Wind Turbine test bed

### *The Sumali Beam*

The Sumali Beam is a 20" by 2" plate with bolt holes regularly spaced along the midline with a 3" center-to-center distance. This structure, however, exhibits very low damping ratios.

A preliminary analysis of this system is detailed in Deaner et al. (2015). This case is useful to demonstrate the difficulty in designing a system that shows an appropriate amount of nonlinearity for both modeling and measurements. Joints with links, such as in the Sumali Beam, tend to have significantly lower damping than more realistic joints.

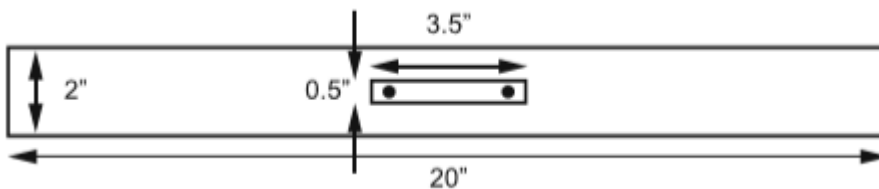


**Figure 13.** The geometry of the Sumali beam with one plate attached

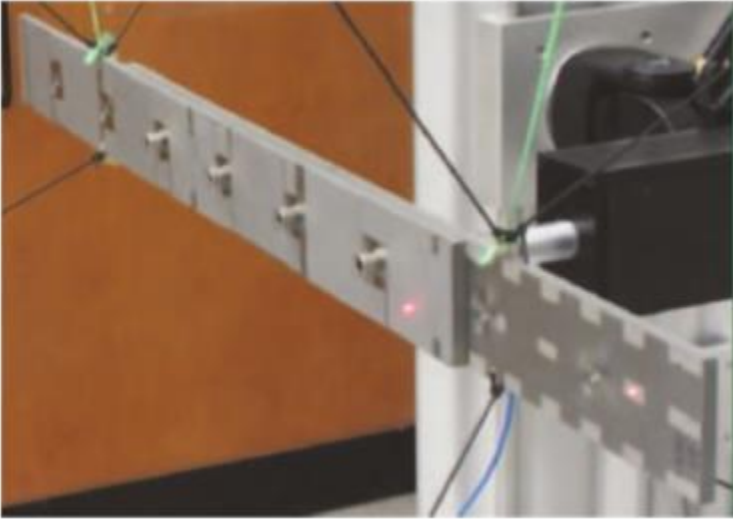


**Figure 14.** Photo of a Sumali beam attached to a second Sumali beam

### *Other Benchmark Systems*

The benchmark systems presented are far from an exhaustive list; however, a growing consensus amongst researchers in this field is that they are appropriate systems to use for benchmark analyses.

From analysis of all of these systems, the essential elements of a good benchmark system are:

1. Simple and cheap to fabricate or easy to purchase.
2. Distributed contact interfaces that support large loads (in contrast to Sumali beam)
3. Easy to model materials or readily available models (in contrast to composites or foam potting).
4. Built in features that allow for a design of experiments to assess effects of the system design on the system dynamics (such as surface roughness or structural stiffness).
5. Simpler structures that allow for smaller/faster computational models.
6. Realistic interface designs for applicability to real systems if possible.

### **Outlook for Adoption of Benchmark Systems**

The recent research on multiple systems highlights that it is possible for meaningful analysis to be conducted on multiple systems and for the resulting lessons to be applied to other systems. In future research, this approach may be greatly beneficial. Additionally, if a benchmark system is selected that provides an in-context application (such as Ampair 600 Wind Turbine), having a complimentary academic system that is simpler to study and model would be essential.

The central question that must be asked before selecting a benchmark system then becomes: “What is the goal of the benchmark analysis?” For projects interested in assessing variability within jointed structures, it will be essential that the system is relatively cheap so that multiple structures can be fabricated (by

contrast, developing a dumbbell system with monolithic substructures may be prohibitively expensive to study variability). If, on the other hand, the goal is to investigate the applicability of new methods to conceptualize energy dissipation in jointed structures, then a dumbbell-like system might be the most appropriate due to the relative ease of modeling. In either case, multiple investigations of the same system facilitate developing a comprehensive understanding of the joint behavior, which is often unattainable by a single lab working in isolation.

## Damping

Damping due to the friction in the interface of the bolted joints dominates the overall damping in these systems; however, the amount of damping due to friction measured in a system can differ by orders of magnitude for experiments on two nominally identical structures. The response of the system in terms of damping and natural frequencies is sensitive to many factors, including the interface condition (e.g. roughness, lubrication, geometrical alignment, etc.)

Damping is a major unknown in dynamics. It controls the amplitude at which a structure vibrates and is thus a major parameter that needs to be modeled in simulations; unfortunately, it is very poorly understood. Furthermore, damping cannot be ignored, for example, if damping is omitted in a simulation and resonance conditions are encountered, then the vibration amplitude is infinite, it is conjectured that joints make a significant contribution to damping.

Damping is a general term for the various mechanisms that result in the permanent removal of energy from a dynamic system. Thus, while most of the energy in a dynamic system is oscillating between kinetic energy and potential energy some of the energy is lost and converted into heat or transmitted out of the system. The loss of energy is modeled as the damping of the system.

In a structure the joints holding the structure's components together are a source of damping. It is suggested that the bolts and the region close to the bolts do not contribute significantly to damping.

Four sources of damping may be identifying in a built-up structure: material damping, damping due to joints, damping within components, and damping due to transmission.

### The damping sites within a bolted joint

Once this question can be answered it will enable simulations and optimizations to be performed so that joint damping can be modeled and designed into a built-up structure.

The general idea from the studies done on a bolted joint is that, the bolts themselves and the joint are in the proximity of the bolt do not cause any damping or at most a damping comparable with material damping. In contrast the joint surface between bolt locations and away from the bolts (i.e., the far field) may, if it slips, cause significant damping.

## Considerations for Measurements of Jointed Structures

The nonlinearity inherent in jointed structures is invariably affected by the boundary conditions, loading conditions, and measurement techniques. Small changes in the experimental setup can significantly affect the measured damping and stiffness of a joint. It is found that the hammer tests performed on the “free” boundary condition monolithic beam has a negligible influence on the system in terms of damping ratio and frequency variation. The time varying changes in stiffening and damping are measured by testing multiple combinations of the experimental setup at different levels of excitation. The results showed that the mirror-like surface finish for the interface has higher damping values compared to the rough surface across multiple bolt torque scenarios (such as preload and tightening order) and modes of vibration. Guidelines for a reliable measurement of features of a mechanical joint are made based on the results of this research.

### Effects of Experimental Setup

To isolate the effects of mechanical joint on a system’s dynamic response is to design the test setup as linear as possible. All test specimens are fabricated from Stainless Steel 304. The basic experimental setup is shown in Fig.10.2, which includes the beam, two bungee cords, two PCB 356A03 Triaxial ICP Accelerometers (Accel), two 356A02 Triaxial ICP Accelerometers used in a second experimental setup, either a PCB 086C03 ICP Impact Hammer or a Bruel and Kjaer PM Vibration Exciter Type 4809 (shaker), LMS 16 Channel Spectral Analyzer, and a modular support rig. The excitation effects are tested in two ways: first with the impact hammer, and second with the shaker.

### Best Practices for Experiments on Jointed Systems

In general, an experimental setup that is as linear as possible is recommended. Specific recommendations from this work are:

1. For impact hammer measurements, the tip and hammer mass do not significantly affect the measurements of damping and stiffness. Thus, the impact hammer configuration should be chosen based on the frequency range of interest.
2. The responses of systems with free boundary conditions created via the use of bungee cords are insensitive to the bungee length, stiffness, and position.
3. The use of accelerometers, even when they are a small fraction of the mass of the system, can significantly affect the measurements of damping and stiffness. If used, accelerometers should be located away from node points, and the number should be kept to a minimum.
4. For shaker excitation, care should be used in selecting an appropriate stinger. Of those tested, the thinner stingers are found to exhibit bending, which results in the appearance of nonlinearities in the system’s frequency responses.
5. The excitation sweep rate, magnitude, and direction are not found to have significant effects for the present system.
6. The conditions of the interface have significant effects on the responses of the system, and future work should aim to quantify the interface conditions thoroughly.

# INTRODUCTION OF CONSTITUTIVE MODELS

## Modeling Considerations

To develop a constitutive model of friction, there are several issues to be considered:

Physical Parameters, Lubrication, State Dependence, Model Implementation

## Friction Models

### 1. Velocity-Based Models

#### 1.1. Coulomb Friction

This model stipulates three principles:

- The area in contact has no effect on the friction force
- If the load of an object is doubled, the friction force is also doubled
- Friction is independent of sliding velocity

To this end, the Coulomb friction model postulates that

$$F = \mu N \quad (1)$$

For a given coefficient of friction  $\mu$  and normal force  $N$ . In order to implement this model numerically, it is often convoluted with a function that either properly assigns the sign of the direction of the force:

$$F = \mu N \operatorname{sign}(v) \quad (2)$$

#### 1.2. Viscous Friction

Viscous friction is typically associated with lubrication and is seen as a term  $cv$  (with viscous coefficient  $c$ ) appended to the Coulomb friction model

$$F = \mu N + cv \quad (3)$$

#### 1.3. Stiction

These models postulate that when an object is at rest, there is a higher (static) friction force needed to initiate motion than the (dynamic) friction force once the object is moving.

$$F \begin{cases} \leq \mu_s N, & v = 0 \\ = \mu N, & v > 0 \end{cases} \quad (4)$$

With static coefficient  $\mu_s < \mu$ .

### 1.4. Stribeck Friction

The previous three models can be combined in multiple ways. Within the Stribeck model, there are four regimes: static friction ( $v = 0$ ), boundary lubrication (low  $v$ ,  $F$  is close to the static friction force), partial fluid lubrication (medium  $v$ ;  $F$  decreases to a local minimum), and full lubrication (high  $v$ ,  $F$  strictly increases). The Stribeck effect is based on the observation that at low velocities, friction forces decrease with velocity, but at some point this trend is reversed and the friction forces increase with velocity once again, as shown in Fig.14.2b

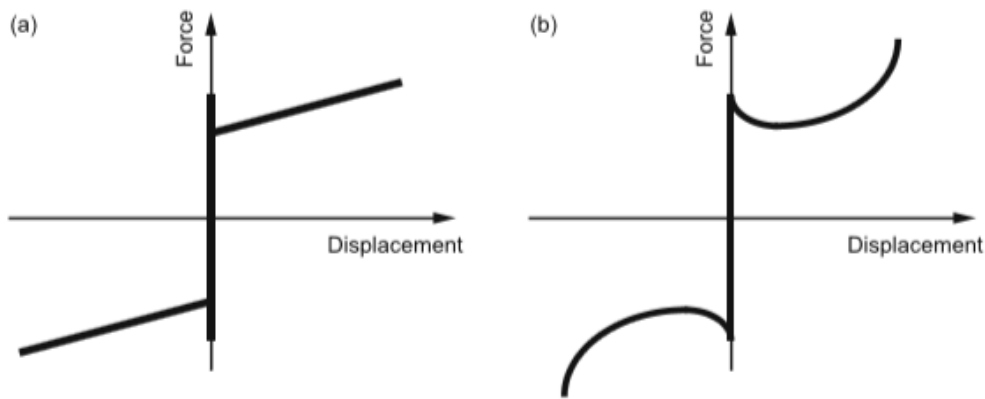


**Figure 15.** Illustrative examples of: (a) Coulomb friction with stiction and viscous effects, and (b) Stribeck friction

## 2. State-Based Models

In contrast to velocity-based models, state-based models require state variable that record the state of the model at previous time-step. In some cases, this could be condensed to a single parameter (such as Jenkin element); in other cases, though, this can require dozens if not hundreds of variables to be tracked (such as with the discretized Iwan model).

### 2.1. The LuGre Model

The Lund-Grenoble (LuGre) friction model (Canudas de Wit et al. 1995; Olsson 1996), also known as the bristle model, is the conceptualization of contact bristles (Fig.16). For simplicity, one set of bristles is assumed to be rigid, and the other set elastic. As asperity distributions are irregular, generally, the LuGre model is based on the average behavior of a collection of bristles that constitute the contact region.

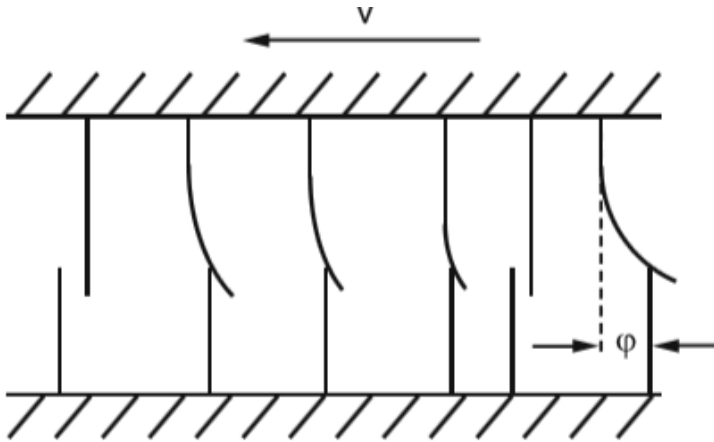


Figure 16. Conceptualization of the LuGre ("Bristle") model

### 2.2. The Jenkins Element

The Jenkin element, attributed to Jenkins (1962), is described by an elastic friction slider, which consists of a frictional element and spring in series as shown in Fig.17. This model is useful for describing some aspects of microslip and macroslip behavior. The model is characterized by a tangential stiffness  $K_T$  and slip force  $F_S = \mu N$ . Once a slip force  $F_S$  is exceeded, the system transitions to pure sliding with force  $F = F_S$ .

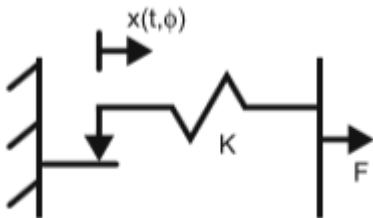


Figure 17. Jenkin Model

### 2.3. The Masing Element

This element is used to refer to a two-dimensional Jenkins element.

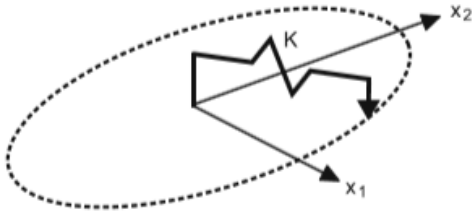


Figure 18. Masing model

#### 2.4. The Iwan Element

Is constructed by a large number of Jenkins elements in parallel, such as shown in Fig.19. The challenge for developing constitutive models in the Iwan element framework is describing the distribution of Jenkin elements (in terms of stiffness and slip forces). The four-parameter Iwan model developed in Segalman (2005) is a discretized representation of the Iwan element in which the properties of the distribution of Jenkins element are represented with four parameters. The tangential stiffness  $K_T$ , the force for inception of macroslip  $F_S$ , the exponent of the energy dissipation per cycle  $\chi$ , and the ratio of Jenkin elements that slip before macroslip to those that slip at macroslip  $\beta$ .

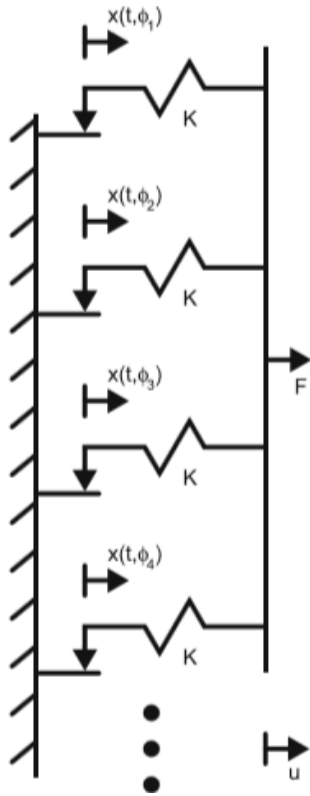
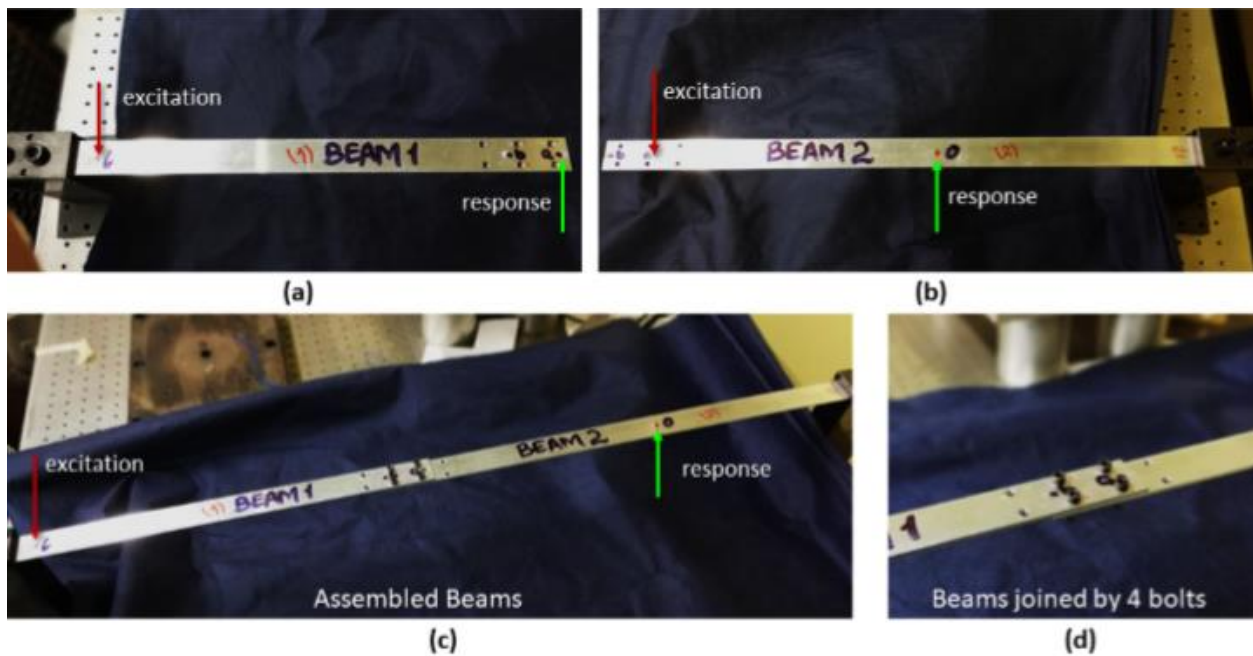


Figure 19. Iwan Model

## TEST CASE: TWO CANTILEVERED BEAMS

The studying structure is made of two cantilevered beams of Aluminum as substructures which are joined at their free-ends when assembled, as shown in Fig.25. The excitation and response points are marked as I on beam-1 and o on beam-2 and “a” and “b” are referring to the interface points. The FRFs are obtained experimentally using impact hammer at the points labelled as “excitation” in the figure and the response is measured at the points labelled as “response” on the individual beams and the assembled structure. The response measurement is performed by Laser Doppler Vibrometers (LDV) measuring only the out-of-plane deflections. The measured FRFs are plotted in Fig.25,26,27. The main response peaks correspond to the bending modes. It is worth-mentioning that the four bolts (steel) for joining are considered as a part of beam-1 and kept tightened on it during measurements acquisition.



**Figure 20.** The experimental configuration of the first test-case. (a) Beam-1 (b) beam-2 (both fixed-free) (c) the coupled beams (d) the joint consisting of 4 bolts. The input and response nodes are also shown in the respective figures. The FRFs obtained on these nodes are subsequently used for FE model updating

Additionally, the beams and the assembly are modelled in the finite element software, ANSYS APDL v17.2 with actual geometric and updated material properties as listed in table 3. The meshing is done with SOLID186 brick element with the mid-side nodes.

**Table 3.** Beam properties

Properties	Beam 1	Beam 2
Material	Aluminium	Aluminium
Dimensions	428*30*3.5	572*30*3.5

# RESULTS

## Case study Beam 1

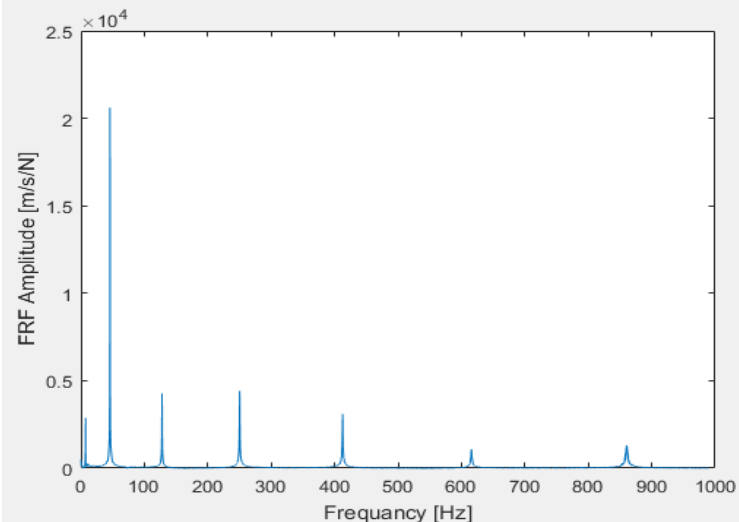


Figure 21. Experimental FRFs of beam 1

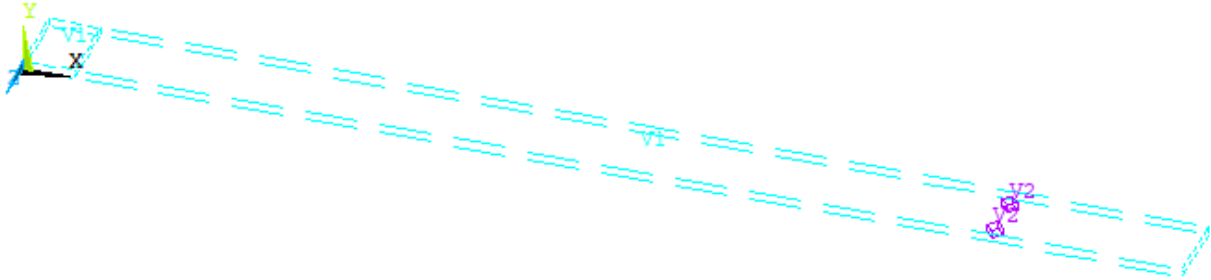


Figure 22. Complete Beam 1 meshed with separate compressed area in the constraint end

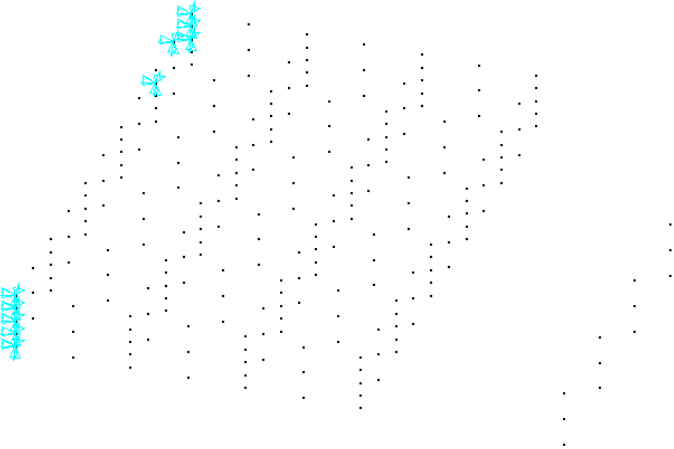
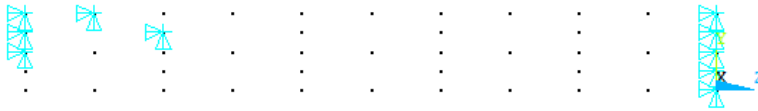
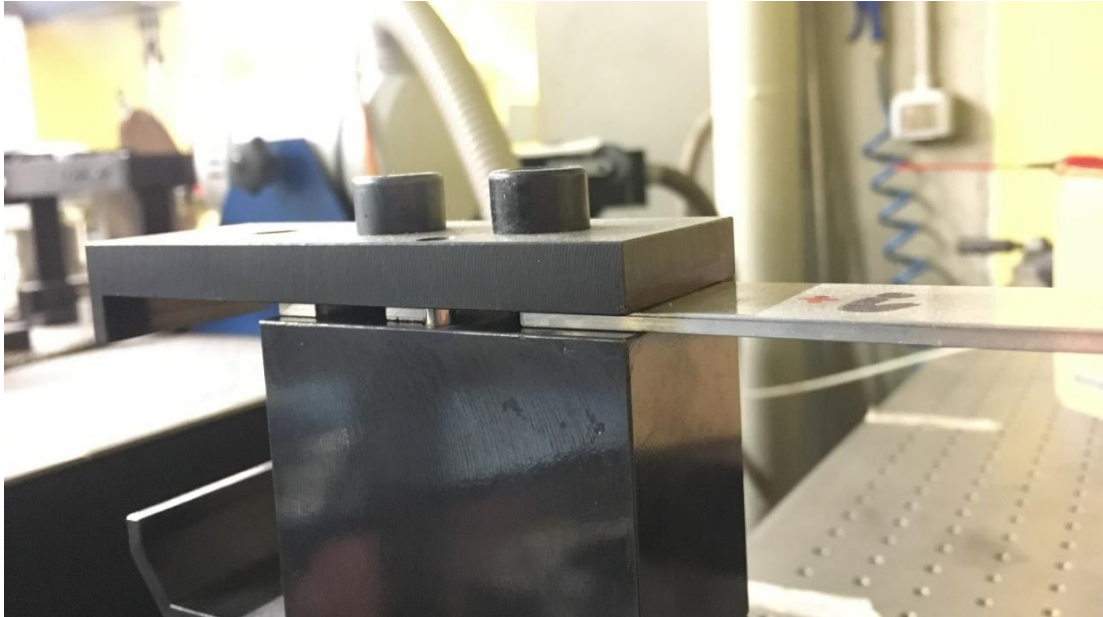


Figure 23. Chosen nodes for the constraint of beam 1



**Figure 24.** Side view of the chosen nodes for the constraint of beam 1



**Figure 25.** Photo of the beam1 constraint end in the rig

**Table 4.** Analytical and Experimental results for beam 1 with four bolts tightened on it

Analytical results with APDL	Experimental results
11.909	10.55
76.394	74.41
117.00	
218.31	216.8
369.63	
432.99	427.73
713.13	705.1
740.10	

Average error percentage between the analytical and experimental methods for the beam with one end constraint and the other end with four bolts mounted on it is 3.7.

Case Study Beam 2

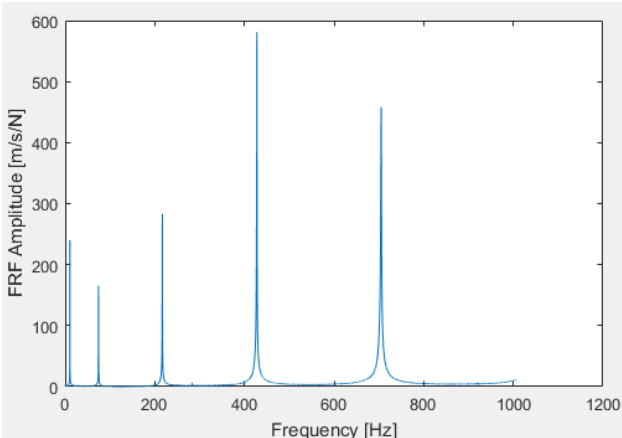


Figure 26. Experimental FRFs of beam 2

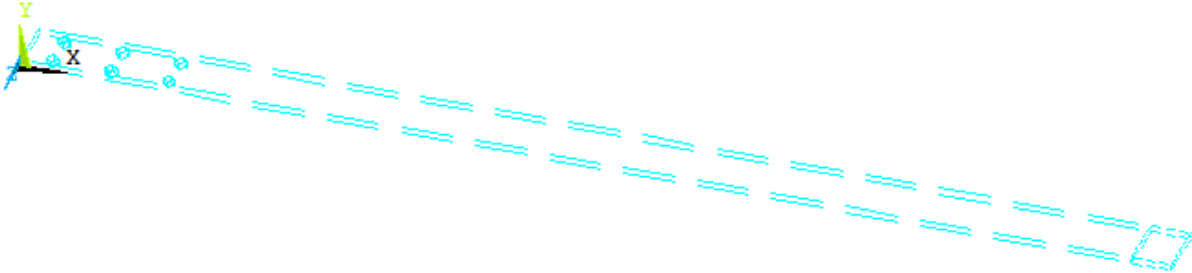
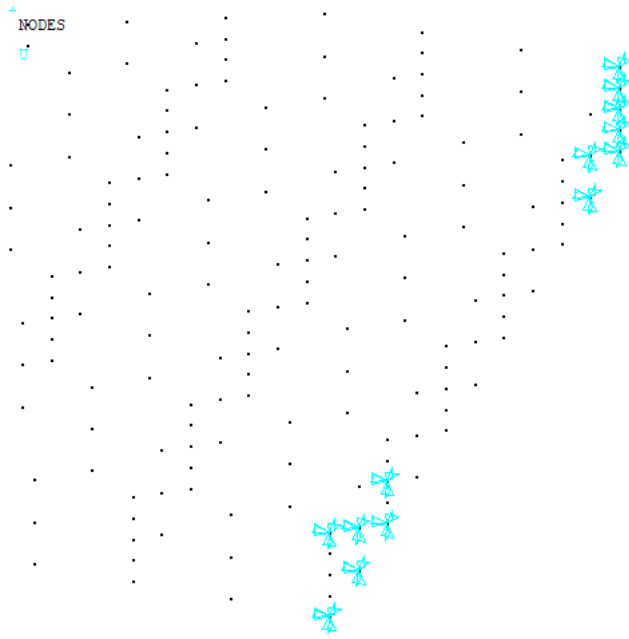
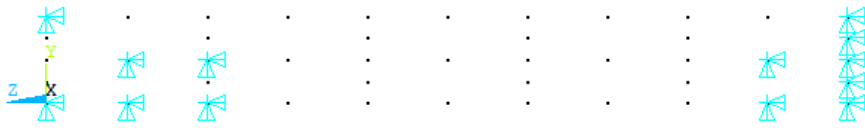


Figure 27. Beam 2 meshed with the separate compressed area in the constraint end



**Figure 28.** Chosen nodes for the constraint of beam 2



**Figure 29.** Side view of the chosen nodes for the constraint of beam 2



**Figure 30.** Photo of the constraint end of the beam 2 in the rig

**Table 5.** Analytical and Experimental results for beam 2

Analytical results with APDL	Experimental results
7.4264	7.41
46.660	45.9
69.952	
130.96	127.92
257.28	250.4
279.50	
426.56	412.7
433.86	
639.47	615.6
839.68	
897.17	860.5

The average error percentage between the analytical and experimental methods for the beam with one end constraint and the other end free is 2.64.

Case Study of Two Cantilever Beams Assembly with four bolts

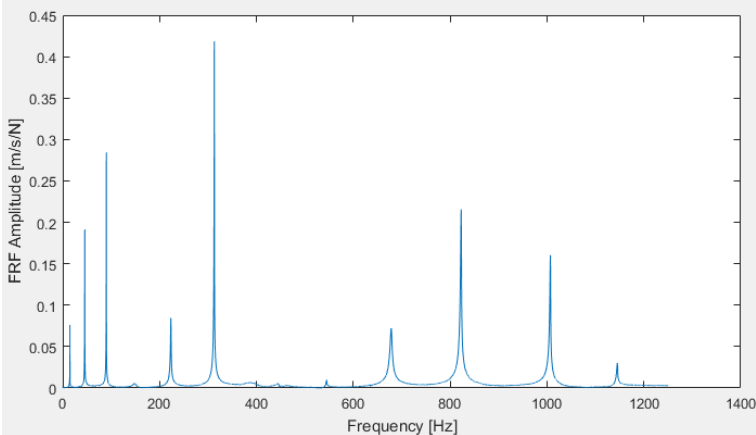


Figure 31. Experimental FRF of the assembly with four bolted joints

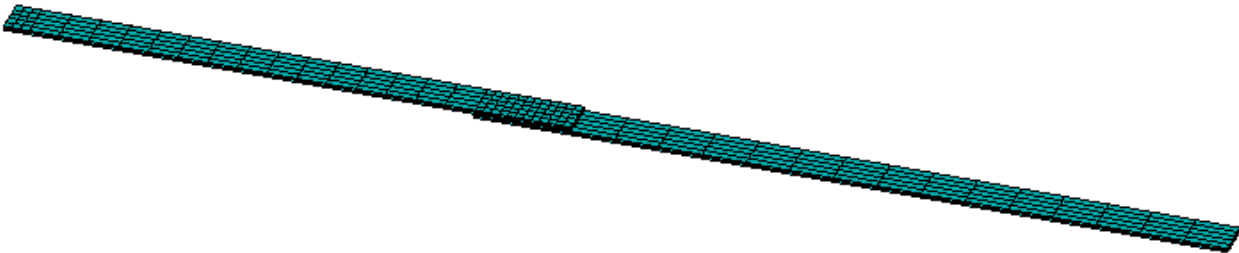


Figure 32. Complete assembly meshed

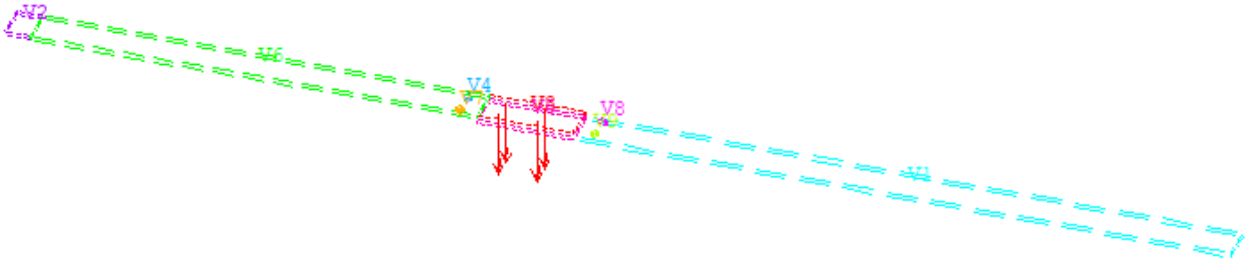
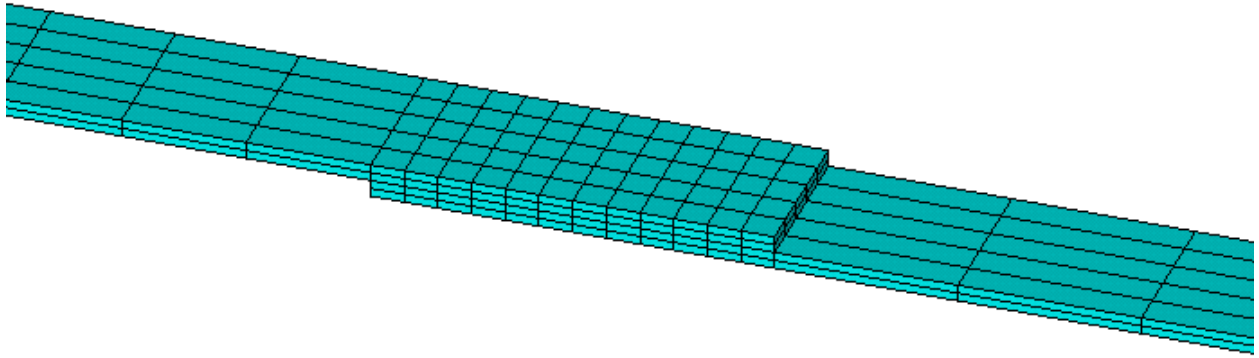
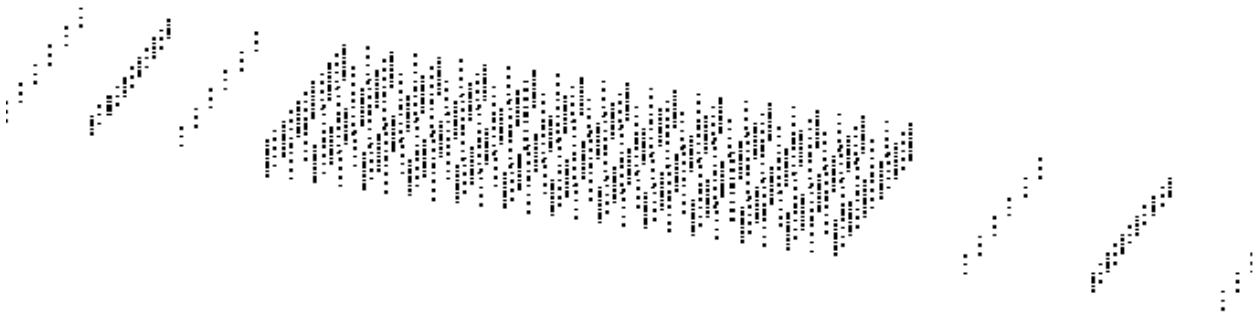


Figure 33. Meshed assembly with symbols



(a)



(b)

Figure 34. (a) Element and (b) Node plot with zoom in the contact volume part

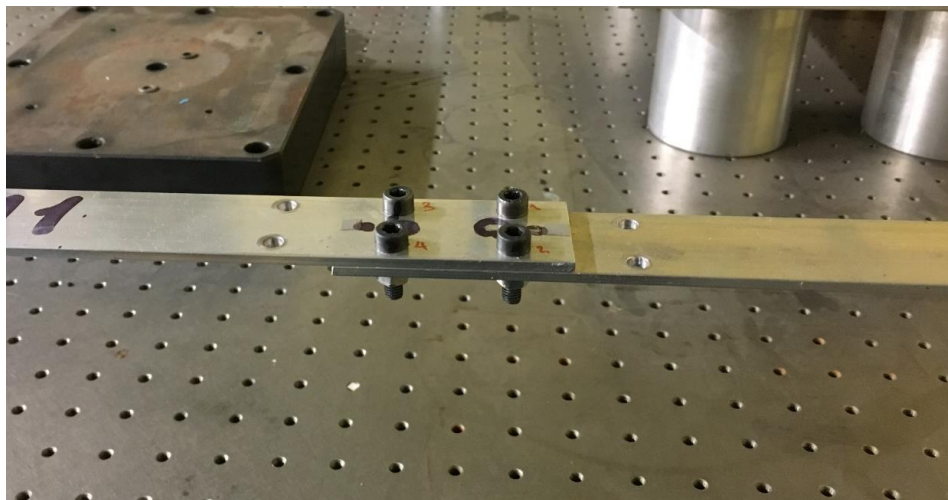


Figure 35. Photo of the contact part with four bolts

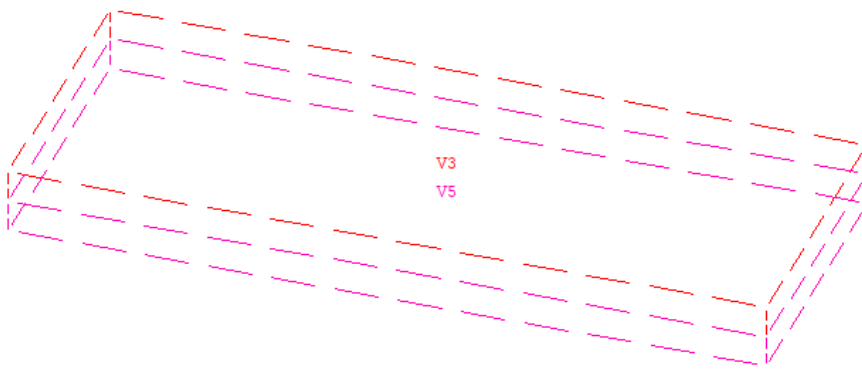


Figure 36. Photo of the contact part with four bolts

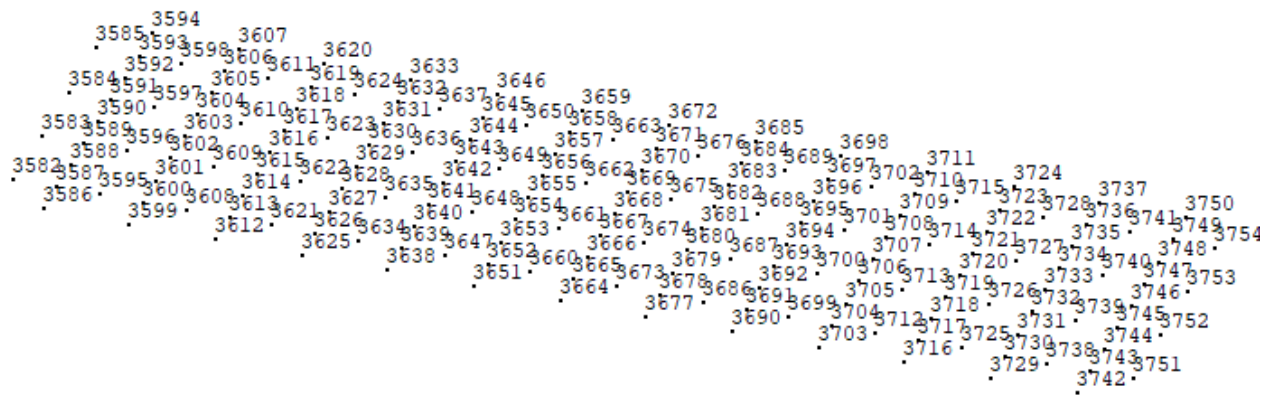
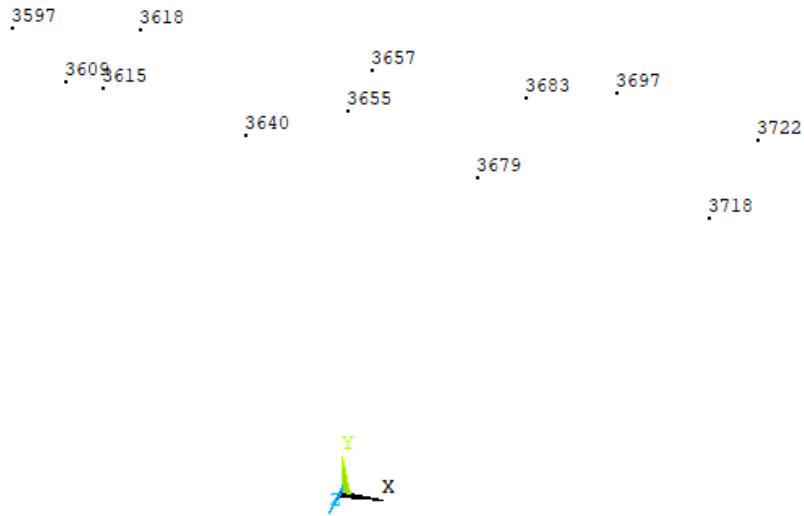


Figure 37. Node numbering in the contact area of two cantilever beams

1  
NODES  
NODE NUM

**ANSYS**  
R17.2  
APR 4 2019  
08:42:24



**Figure 38.** Selected nodes for merging in the contact area of two cantilever beams with four bolted joints mounted

**Table 6.** Analytical and Experimental results for the assembly with four bolts mounted it

Analytical results with APDL	Experimental results
16.180	14.844
49.799	45.51
94.684	90.04
154.53	148
164.24	
242.40	223.24
317.72	313.085
345.29	
411.80	387
451.19	445
586.57	544.9
718.74	678.32
726.56	
868.19	822.65
903.88	
1031.8	1007
1099.6	
1164.5	1145.3
1376.1	
1420.7	

At the end there is an average error of 5% between the experimental and analytical methods results.

## IWAN MODEL INTRODUCTION

Structures with mechanical joints are not easy to model accurately; even if the natural frequencies of the system remain constant, the damping introduced by the joint is often depending nonlinearly on amplitude. This approach assumes that the mode shapes of the structure do not change significantly with amplitude and there is negligible coupling between modes. The nonlinear Iwan joint model has had success in modeling the nonlinear damping of individual joints and is used as a modal damping model. The proposed methodology is evaluated by simulating a structure with a small number of discrete Iwan joints (bolted joints) in a finite element code. A modal Iwan model is fit to simulated measurements from this structure with the assessment of the modal model. The same methodology is then applied to actual experimental hardware with a similar configuration. The proposed approach captures the response of the system in both cases (microslip and macroslip), especially at up to moderate force levels when macroslip does not occur.

Macroslip occurs when the stick region vanishes and larger slip displacements are possible.

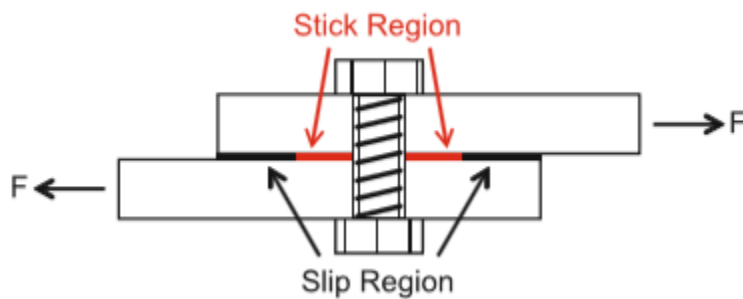


**Figure 39.** Contact and slip regions are shown for a mechanical joint undergoing microslip (Segalman 2001)

For some structure it may be possible to represent groups of joints as a single interface, or to exploit symmetries to replicate one joint many times, but these types of approaches have not yet been thoroughly developed. On the other hand, when a small number of modes are active in a response, some measurements have suggested that a simpler model may be adequate. Segalman investigated the idea of applying the four-parameter Iwan model in a modal framework in Segalman (2010), in which simulated measurements are used to deduce the modal Iwan parameters for two simple spring mass systems and compared to the more rigorous approach where each discrete joint in the system is treated separately.

Providing a basic introduction, an analytical case study and a review of recent experiments that support the framework of modal modeling for structures with discrete Iwan joints; First, a finite element model of a structure with four discrete Iwan joint is used to simulate an experiment and after that the simulated response data is used to deduce a set of modal Iwan parameters. The approximation of the responses of the structure with individual discrete joints with one modal Iwan model per mode are then carefully compared to ascertain the degree to which the simpler modal model can capture the response of the higher fidelity model. At the end, experiments on an assembly of stainless steel beams and automotive catalytic

converters are summarized. Both cases result that the modal Iwan model can describe the measured response with very good accuracy.

### Four-Parameter Iwan Model

It is a nonlinear energy dissipation model and Mathematically, the four-parameter Iwan model is represented as

$$F_{Iwan} = \int_0^{\infty} \rho(\varphi) (u(t) - x(t, \varphi)) d\varphi \quad (5)$$

The four-parameter population density function which is a power law representation and describes a distribution of Jenkins elements developed in Segalman (2005) has the form:

$$\rho(\varphi) = R \varphi^{\chi} (H(\varphi) - H(\varphi - \varphi_{max})) + S \delta(\varphi - \varphi_{max}) \quad (6)$$

Where,  $H(0)$  is the Heaviside step function,  $\delta(0)$  is Dirac delta function, and the four parameters that characterize joint include  $R$ , which is associated with the level of energy dissipation,  $\chi$ , which is directly related to the power-law behavior of energy dissipation,  $\varphi$ , which is equal to the displacement at macroslip, and the coefficient  $S$ , which accounts for a potential discontinuous slope of the force displacement plot when macroslip occurs.

Which yields the general form of hysteresis loop shown below (Fig. 20). The parameters  $R$  and  $S$  are both calculated from four model parameters ( $K_T, F_s, \beta, \chi$ ).

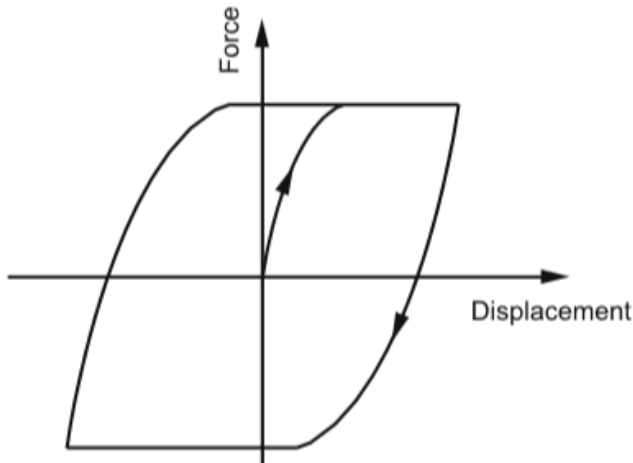


**Figure 40.** Illustrative drawing of a typical hysteresis curve for a four-parameter Iwan model described by Segalman (2005)

The four parameters  $R, \chi, \varphi, S$  are converted to more physically meaningful variables  $K_T, F_s, \chi, \beta$  in Segalman (2005) and Segalman and Holzmann (2005):  $F_s$  is the joint force necessary to initiate macroslip,  $K_T$  is the stiffness of the joint,  $\chi$  is directly related to the slope of the energy dissipation in the microslip regime, and  $\beta$  relates to the level of energy dissipation and the shape of the energy dissipation curve as the macroslip force is approached. However, each joint may require a unique set of these parameters, so many joint

parameters need to be deduced and corresponding discrete joint models increase the cost of transient simulations in the structural-level finite element model.

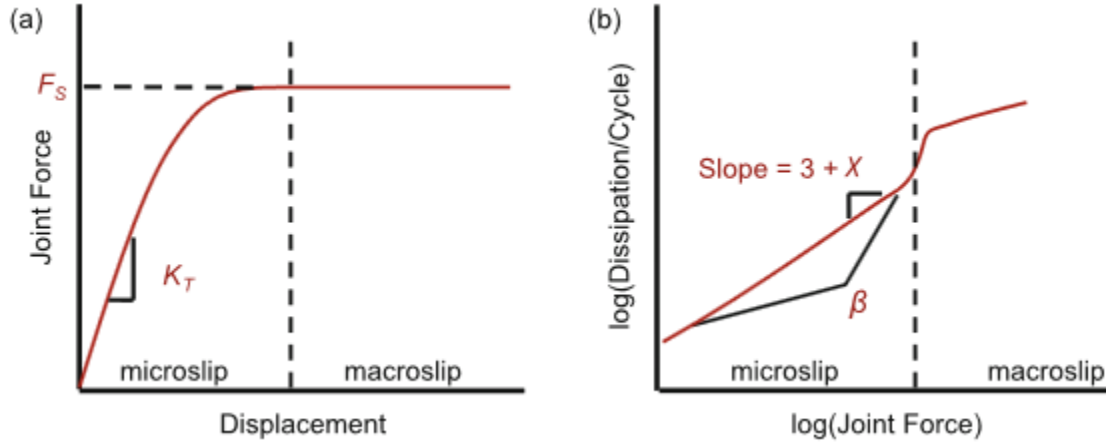


**Figure 41.** (a) Both macroslip force ( $F_s$ ) and joint stiffness ( $K_T$ ) can be found from the force displacement relationship of the joint. (b) The  $X$  value is found from the slope of the dissipation and the  $\beta$  value is a measure of dissipation level and shape of the dissipation curve

This new set of parameters can be deduced from the two plots Fig.41. There are a variety of methods that could be used to find the energy dissipation and frequency by estimating them from the free response of each mode of interest. Once these are known, the Iwan parameters can be determined using nonlinear optimization as discussed in Segalman (2005), graphically, or through some combination of the two. This work focuses on the graphical approach.

For a system where the damping is strictly due to the four-parameter Iwan model, the equation becomes:

$$M \ddot{x} + K_{\infty} x = F_X + F_J \quad (7)$$

With linear mass  $M$  and linear stiffness  $K_{\infty}$  matrices of a finite element model, and vectors of external forces  $F_X$  and nonlinear joint forces  $F_J$  applied to the structure which has nonzero entries corresponding to the two ends where the joint is attached to the finite element model and depends on the history of displacement at those points. Matrix  $K_{\infty}$  has no contributions from the joint locations; even the linear portion of the joint response is captured in  $F_J$ .

The four-parameter Iwan model has been implemented to predict the response of structures with a small number of discrete joints (Allen and Mayes 2010; Segalman and Holzmann 2005). However, each joint may require a unique set of parameters  $\{K_s, F_s, X, \beta\}$  so many joint parameters need to be deduced and corresponding discrete joint models increase the cost of transient simulation in the structural-level finite element model.

*The Iwan Model and the Four-Parameter Iwan Model*

The parallel-series Iwan model (Iwan 1966, 1967) is a phenomenological model of yielding and microslip in which the physical process is represented by the stick-slip behavior of a parallel array of Jenkins elements with different slip threshold. Its global dynamic behavior is fully described by the frictional properties of the Jenkins elements and the distribution  $\rho(\phi)$  of Jenkins elements slipping under a displacement  $\phi$ . Adopting the dimensionless formulation of Segalman (2005), it can be shown that the force  $F(t)$  is:

$$F(t) = \int_0^{\infty} \rho(\varphi) (u(t) - x(t, \varphi)) d\varphi \quad (8)$$

For a displacement  $x(t, \varphi)$  at time  $t$  of the Jenkins element with slip displacement  $\phi$ .

Assuming that these elements are massless, that the friction force is constant during slip, and that the static and dynamic coefficients of frictions are equal (normalized).

$$\dot{x}(t, \varphi) = \begin{cases} \dot{u}(t) & \text{during slip} \\ 0 & \text{during stick} \end{cases} \quad \text{Slip onset} \quad \|u(t) - x(t, \varphi)\| = \varphi$$

Under an oscillatory displacement  $u(t)$ , the maximum applied force  $F_0$  is (Segalman 2005)

$$F_0 = \int_0^{u_0} \varphi \rho(\varphi) d\varphi + u_0 \int_{u_0}^{\varphi_{max}} \rho(\varphi) d\varphi \quad (9)$$

Where  $\varphi_{max}$  denotes the displacement at which macroslip occurs. The general dissipation of the whole system under the harmonic motion is obtained as (Segalman 2005)

$$D = \int_0^{u_0} 4(u_0 - \varphi) \varphi \rho(\varphi) d\varphi \quad (10)$$

Proceeding with two differentiations of Eqs. (9) and (10) with respect to  $u_0$  yields

$$\frac{\partial^2 F_0}{\partial u_0^2} = -\rho(u_0) \quad (11)$$

and

$$\frac{\partial^2 D}{\partial u_0^2} = 4u_0 \rho(u_0)$$

From which it is found that

$$\frac{\partial^2 D}{\partial u_0^2} + 4u_0 \frac{\partial^2 F_0}{\partial u_0^2} = 0 \quad (13)$$

Subsequently it is clear that there is a relationship between  $F_0$  and  $D$  implied by the Iwan modeling assumption which is a reflection of the dependence of both of these quantities on the single distribution  $\rho(\phi)$ .

The four-parameter Iwan model introduced in Segalman (2005) is a specific version of the general one above in which the distribution  $\rho(\phi)$  is expressed as

$$\rho(\varphi) = R \varphi^\chi (H(\varphi) - H(\varphi - \varphi_{\max})) + S\delta(\varphi - \varphi_{\max}) \quad (14)$$

where  $H(0)$  and  $\delta(0)$  are the Heaviside and Dirac delta functions. Note that the last term in the above equation is introduced to model the occurrence of the macroslip at  $\varphi = \varphi_{\max}$ . Introducing Eq. (14) in Eqs. (9) and (10) leads to

$$F_0 = K_T u_0 - \frac{(R u_0^{\chi+2})}{(\chi+1)(\chi+2)} \quad (15)$$

With tangent stiffness

$$K_T = S + \frac{R\varphi_{\max}^{\chi+1}}{\chi+1} \quad (16)$$

And dissipation

$$D = \frac{4R u_0^{\chi+3}}{(\chi+3)(\chi+2)} \quad (17)$$

Finally, the stiffness is defined as

$$K = \frac{F_0}{u_0} = K_T - \frac{R u_0^{\chi+1}}{(\chi+1)(\chi+2)} \quad (18)$$

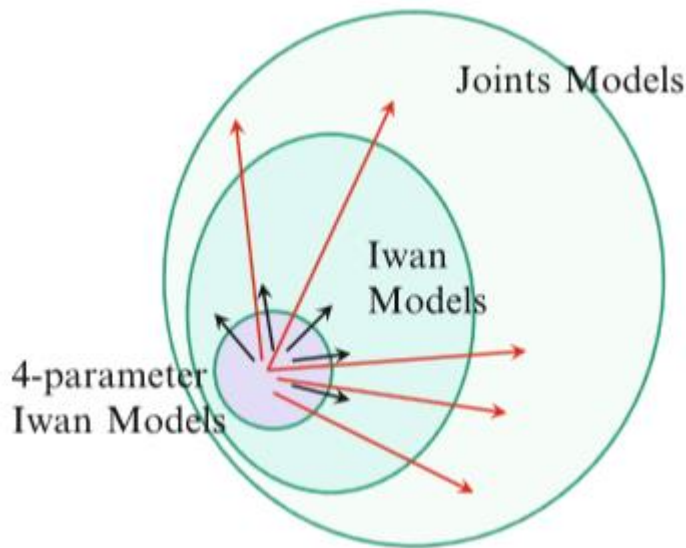


**Figure 42.** Extensions of the four-parameter Iwan models

## Extended Iwan-Type Models: Five-Parameter Iwan-Type Model

The four-parameter model described in the previous section is limited in its applications and does not provide a single modeling of the force in the joint versus displacement as would be required if the joint was part of the structure being excited. Hence, another approach to have a better representation and to reduce epistemic uncertainty with stochastic deviations of the model and to broaden the modeling area of the four-parameter Iwan model is necessary. Additionally, in the referring model it is allowed to have static and dynamic coefficients of frictions,  $\mu_s$  and  $\mu_d$  different from each other. It is further assumed that when slip is initiated in a Jenkins element, the force it carries drops suddenly from  $\mu_s N$  to  $\mu_d N$ , and it continues to carry until stick occurs. Therefore, we can decide the slipping Jenkin elements carry forces equal to  $\theta$  times the forces they would carry if  $\mu_s = \mu_d$

$$\theta = \frac{\mu_d}{\mu_s} \leq 1$$

Eqs.(35.1) and (35.2) are still valid, but the slip occurrence is discontinuous

$$\begin{aligned} \text{Slip onset} \quad & \|u(t^-) - x(t^-, \varphi)\| = \varphi \\ \text{After slip} \quad & \|u(t^+) - x(t^+, \varphi)\| = \theta\varphi \end{aligned}$$

In harmonic motions, the peak value of the force  $F_0$  becomes

$$F_0 = \theta \int_0^{u_0} \varphi \rho(\varphi) d\varphi + u_0 \int_{u_0}^{\varphi_{max}} RO(\varphi) d\varphi \quad (19)$$

Instead of Eq. (9). The dissipation is obtained, as done for Eq. (10), by determining the area of the hysteresis loop. We obtain

$$D = \theta \int_0^{u_0} 4(u_0 - \theta\varphi) \varphi \rho(\varphi) d\varphi + \int_0^{u_0} (1 - \theta)^2 \varphi^2 \rho(\varphi) d\varphi \quad (20)$$

Following the arguments of Segalman et al. (2009), Segalman (2005), and Segalman and Starr (2004), it is adopted here as in the four-parameter Iwan model, i.e., Eq. (14). Integrations yields

$$F_0 = K_T u_0 - \frac{R[\chi+2-\theta(\chi+1)]}{(\chi+1)(\chi+2)} u_0^{\chi+2} \quad (21)$$

Considering the previous definition of  $K_T$ , i.e., Eq.(16) and

$$D = \frac{R[2\theta(\chi+4)+(1-3\theta^2)(\chi+2)]}{(\chi+3)(\chi+2)} u_0^{\chi+3} \quad (22)$$

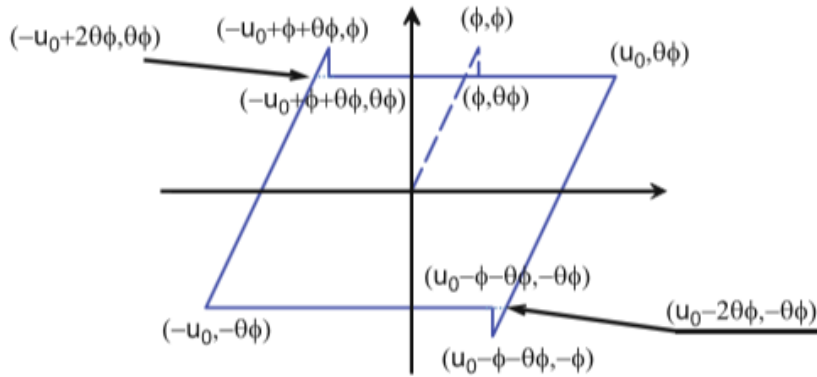


**Figure 43.** Hysteresis loop for the proposed five-parameter Iwan model, shown for  $\theta=0.8$

While the model proposed here involves five parameters,  $\theta$ ,  $R$ ,  $\chi$ ,  $S$ , and  $\varphi_{max}$ , its behavior prior to macroslip is dictated by four parameters:  $\theta$ ,  $R$ ,  $\chi$ , and  $K_T$ , consistently with four-parameter model, which only involved three parameters:  $R$ ,  $\chi$ , and  $K_T$ .

To give an example modeling of Sandia Joints Data with the above model of equations (21) and (22) through the minimization of the error of is quite successful, leading to a good match of both stiffness and dissipation.

The overall focus of this part of investigations done before was the development and validation of stochastic Iwan-type models for the characterization of a particular class of bolted joints from available experimental data with broad scatter on its stiffness and dissipation behavior. The four-parameter parallel-series Iwan model of Segalman (2005) was first extended to include not only differing parameters in the modeling of the stiffness and dissipation properties but also differing static and dynamic coefficients of friction leading to the introduction of the fifth parameter  $\theta$  (the “five-parameter model”). The additional modeling flexibility permitted the last model led to a good match of both dissipation and stiffness data. Accordingly, this model was used to construct the desired stochastic model of the joint by randomizing only its parameters. The statistical distribution of these parameters were selected on the basis of maximum entropy arguments while satisfying the physical constraints of the model was identified using an approximate maximum likelihood strategy defined on the space of the random Iwan model parameters. Finally, the experimental data was found to fit well within the uncertainty band corresponding to the 5<sup>th</sup> and 95<sup>th</sup> percentiles of the predictions obtained with either model which well supports their adequacy. The methodology developed in these steps is expected to be applicable to other joint and/or joint models.

## The Next Generation of Joints Research

Stemming from the notion that the response of a jointed structure may depend upon quantities that are outside of a designer's control (such as grain distribution), these quantities should be accounted for using uncertainty characterization techniques for epistemic uncertainty. Other parameters, particularly as related to geometry and material properties, should serve as direct inputs to an ideal joint model. Related to this, the conceptualization of parameters as being deterministic is limiting our approach to modeling jointed structures. It must be recognized that all parameters within a model are stochastic by nature, and the techniques for measuring and incorporating them into a model must reflect this.

### On Numerical Modeling

With the advance of Iwan and other hysteretic friction models, there now exist multiple high fidelity constitutive representations of the hysteresis observed in frictional events. However, at the same time, it has become apparent that an accurate (calibrated) constitutive model of a hysteretic process is not enough for developing an accurate numerical model of a jointed structure. Due to the coupling of structures and modes inherent to nonlinearities and to the local kinematics, careful attention to the spatial modeling and coupling is needed. It is not enough to calibrate a friction model without considering the effects of the local kinematics within a joint. Instead, as new insights are gained into how to couple two different substructures at a jointed interface, the ideal constitutive model may, in isolation, not resemble the system's response, which is a product of contact across an entire flexible interface, not just a point. Thus, a reasonable hypothesis is The spatial modeling of interactions within a jointed interface is as important, if not more so, than the constitutive modeling of the hysteresis exhibited by the system.